DESIGN AND IMPLEMENTATION OF PEAK CURRENT DETECTION BASED MULTILEVEL INVERTER FOR PV ARRAY FED BLDC MOTOR DRIVE FOR IRRIGATION PUMP APPLICATION

Dr S.Hussain Vali, Kola Venkata Siva Kalyan, V.Rafi, Department of Electrical and Electronics Engineering, JNTUA College of Engineering Pulivendula, Kadapa, India.
Dr Kurakula Vimala Kumar, Department of Electrical and Electronics Engineering, JNTUK University College of Engineering, Narsaraopet, India.
Corr.author mail: vempallerafi@gmail.com

Abstract— In this article, 5- level cascaded multi-level inverter (MLI) with Adaptive neuro –fuzzy inference system ANFIS controller, the solar PV array out put to use the maximum peak of the output to use the process. The photovoltaic system actually output is DC and then covert into AC and connected to multi-level inverter (MLI),The multi-level inverter (MLI),electrical energy and converted into mechanical energy to the BLDC motor output to the water pumping apparatus. The purpose of the system, to using the multi –level inverter harmonic distortions will be reducing output wave forms are smoothing. In this type of 5-level cascaded multi –level inverter, because levels increased and efficiency is also increase then magnitude increase shape is smooth. The back emf voltages, uses reference signal, used to carrier base signal compare to then pulses generated to the system, and INC method are also used comparisons ,the MPPT output pulses connected to the gate pulse generated .Incremental conductance duty cycle and ANFIS control used pulse generated this process is a ANFIS based Incremental method. Using MATLAB software are taken for the output of the solar PV array in the two conditions are taken steady state and dynamic states.

KEY WORDS —Peak current detection-based starting, incremental conductance (INC) maximum power point tracking (MPPT) algorithm, permanent magnet brushless direct current (PMBLDC) motor driving, position sensor-less control, and water pumping.

1. INTRODUCTION
Costs associated with solar (PV) arrays has decreased significantly over the past ten years together with the growing loss of fossil fuels ,generating solar power one of the most dependable non-renewable energy sources. Water pumping is extremely necessary since Water shortages are impacting a significant the effect on agriculture and the provision of drinkable water, particularly during the summer in rural parts of India and the remaining globe with low water tables. The ecology is harmed by the diesel-powered pumps' ongoing operating costs. They are becoming less significant, whereas solar-powered water pumps, especially those used for irrigation, are becoming more significant. Hand pumps for potable water are now also being replaced with motor-coupled water pumps in rural regions. In order to manage the irrigation pump powered by a PV array is driven by a BLDC motor, peak current detection starting is used. [1].a single-stage solar array supplied by two inverters,pumps with an open-end winding induction motor drive. An individual switch's design PFM+PWM controlled DC/DC converterfor a system using PV batteries. This system uses a low-cost, high-efficiency, and long-lasting converter to power an independent solar water pump. [2-4].
From almost zero to high speeds, the BLDC motors may be controlled without using sensors. With few components, this BLDC motor is suitable for all speed ranges. For home appliances, sensor less DC motors with estimated torque constant. [5-7].
High-speed BLDC motors for aerospace applications using a buck converter-based design for three-phase H-bridges brushless direct current motors with sensor-free commutation that are printed circuit. PV-powered water pumping with BLDC motor drive supplied via buck-boost converter. [8-10].
Pumping of water device powered by a straightforward brushless DC motor. Utilizing a fuzzy inference system with adaptive neuros,for freestanding solar PV power systems, a MPPT system.

Performance evaluation of MPPT methods based on neural networks and fuzzy logic for solar PV systems. [11-13].

Surface permanent-magnet BLDC motors without position sensors are started using a revolutionary technique for reciprocating compressors. Water pump powered by a single stage brushless DC motor fueled by solar PV. Increased conductance with better performance at lower cost PV MPPT method.[14-16].

Using an estimated high starting current and the current study examines thefluid without jerking, intermediately stable sensor-less the beginning of a PMBLDC motor by modifying the transit period to maintain the beginningcurrent usingthe required range.Moreover, the article provides a thorough study of running controls without position sensors in light of the widespread adoption of these controls with lowphase current detectors. The benefits within this control arewhich are listed.

1)Peak current detection-based beginning algorithm is used by the drive to manage the initial peak current.2) Due to great motor and system efficiency, the PV array's electrical rating is decreased, which decreases the overall cost.3) The situation sensor-lesscontrol produces the driving heavy dependable in severe weather.

2. SYSTEM CONFIGURATION

Fig. 1shows this water pump system powered by a solar PV array with BLDC motors. The VSI supplying the BLDC-powered pump is connected to the solar PV array. The solar power system's output has a series diode connected to stop current from flowing in the other direction. The INC algorithm was used to acquire the MPPT forthe PV solar system. By sensing the PV voltage and PV current, the VSI manages the MPPT. The system is devoid of position sensors. The 120° conduction mode is used to run the VSI.
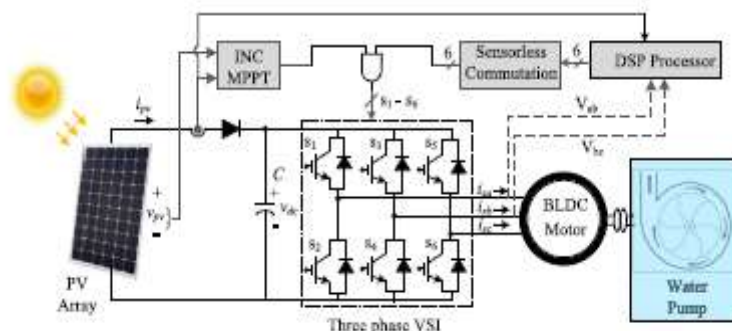

Fig. 1. System configuration of position sensorless brushless DC motor drive.

3. DESIGN SPECIFICATION AND SIZING

A PV array's right design is crucial for the BLDC motor drive based water pump. A 4-pole, 3000-rpm, 1.3-kW BLDC motor is used to power the water pump. The system is made to maintain the minimal speed necessary to ensure that water pumping is unaffected by the fast variations in solar insolation. Table I provides a list of the brushless dc motor's precise electrical parameters**.**

3.1. Solar PV Array Sizing

A sun irradiation of 1000 W/m2 under standard test circumstances is taken into consideration for the steady-state optimal performance [17].

Despite the fact that the motor has a power rating of 1.3 kW, the solar PV array's power rating is taken to be 1.5 kW in order to cover the system's intermediary losses.

Complete load and 1000 W/m2 radiation, the PV array's voltage is taken to be 310 V.

It is done as follows to estimate capacitor C:

$$C = \frac{I_{dc}}{6*\omega*\Delta V_{dc}} \qquad\qquad ………(1)$$

$$I_{dc} = \frac{P_{mpp}}{V_{dc}}$$

$$\omega = \frac{2*\pi*N}{60} = \frac{2*\pi*3000}{60} = 314.159\frac{rad}{sec} \; ;$$

N is equal to 3000 rpm, the motor speed for pumping water.2% is regarded as the value of V dc, which is the dc-link ripple voltage, As a result, the anticipated value of the dc-link capacitance is

$$C = \frac{I_{dc}}{6*\omega*\Delta V_{dc}} = \frac{4.83}{6*314.159*0.02} = 500\mu F$$

The ultimate choice is C = 470 F since voltage at the dc-link has the VSI output voltage's sixth harmonic component.

3.2. Water Pump Design

Based on the basic pump-power connection [18],when calculating the motor shaft power or pump input power,

$$P = \frac{Q*H*SG}{367*n} \qquad\qquad ……….(2)$$

Where, P is power of the pump shaft in kW, Q is water flow rate in m3/h, H is dynamic water head ,SG is water specific gravity , n is pump efficiency.

4. CONTROL ALGORITHM

Control system divided into three primary parts: Sensorless BLDC motor position estimation, MPPTcontrolling a solar PV array with point controls, andElectronic commutation of the BLDC motor is controlled by VSI switching pulses.Next section goes into further information about control algorithms.

4.1 Position sensorless control

 BLDC motor, the switching point occurs during the time the back EMF of the incoming the phase is equivalent to back EMF of the outgoing phase. At this moment of commutation, the back EMF of the incoming phase reaches its greatest value, as well as the back EMF of the departing phase begins to declinecompared to its highest value.At the precise moment of commutation, the line's back EMF is zero and recently altered from being negative to being positive. The levels of the phase back EMFs are the incoming and outgoing likewise equal.Two phases of a BLDC motor conduct concurrently while third phase is left floating. One conducting phase and one floating phase are turned on and off at every 60-degree interval. current flowing through phase a constant and the currentflowing through phase b is zero when considering the transition of conduction from the a-c to the b-c phases at the start of the commutation, or $i_a = I$ and $i_b = 0$, respectively.Phase a's current is now zero, while phase b's current is fixed, or ia = 0 and ib = I.The average current flowing through the inductor remained constant throughout the switching cycle, which is supported by the following calculations, hence the inductor experiences no voltage loss. At the beginning of the commutation, phase a and   b voltages are determined by the following formulae:

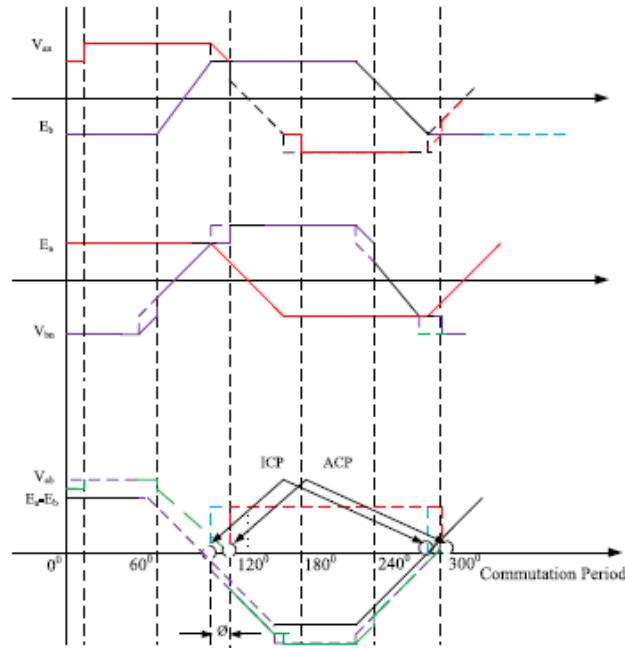$$V_{an} = Ri_a + e_a \; ; \; V_{bn} = e_b . \qquad\qquad ………(3)$$

The line voltage is therefore stated as

$$V_{ab} = Ri_a + (e_a - e_b). \qquad\qquad ………(4)$$

Neglecting the Ria drop, the voltage of the line drops to zero at the point of commutation, giving the ideal commutation instant, which is ea = eb, when considering (3), which becomes
$e_a = e_b$, $V_{an} = V_{bn}$.   ………(5)
It is done directly to the line voltage. In place of the line back EMFs in this technique considering that the line back EMFs arenot readily accessible and winding resistance drop is ignored. At the motor terminals, the line voltages are easily measurable. The commutation moment is considered to occur at the line voltage zero crossing point. **Fig. 2** provides a description of the previously indicated control method.

ICP= Ideal Commutation point
ACP= Actual Commutation point
Fig. 2. Estimation of commutation point from back EMF

4.2. Control of Maximum Power Point

The intermediate converter is run at the solar PV array's optimal operating point using the INC [19] based MPPT control to harvest the most power possible. The slope of the solar P-V characteristics is used by the INC-based method to estimate the direction of the perturbation. The flow diagram is elaborated in Fig. 3.This method indicates that the slope of the aforementioned curve is zero at MPP. When it is on the left, it is positive; when it is on the right, it is negative. The following equations provide a description of this procedure:

$$\frac{dP_{pv}}{dv_{pv}} = 0, \text{ at maximum power point} \qquad\qquad \text{………} (6)$$

$$\frac{dP_{pv}}{dv_{pv}} > 0, \text{ at the left's optimal operating position…… } (7)$$

$$\frac{dP_{pv}}{dv_{pv}} < 0, \text{ when the rightmost functioning point is present. …… } (8)$$
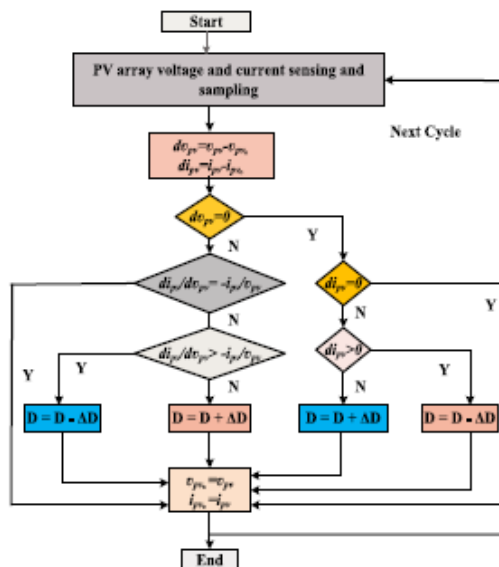

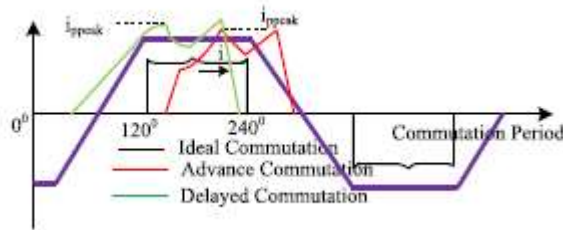**Fig. 3.** State flow of incremental conductance.

Fig.4. Peak current detection

The current is seen to have a peaky edge. Additionally, it has been shown that with advanced commutation, the rising of phase current occurs prior to the beginning of true commutation. For the advance commutation process as well, a significant peaky current is seen.As a result of the aforementioned circumstance, the phase current experiences an unwelcome high peak, damaging both the drive and the motor windings. As a result, phase current experiences a significant inrush surge during startup. The first high current shoot-up caused by faulty commutation is reduced using the beginning approach described in this article. After phase current detection, the average phase current (I_{avg}) of a phase is determined by a non-commutated phase's current being averaged immediately after the temporary stage of commutation. Over current peak (i_0) is estimated as 110%−120% of I_{avg}. Comparison between sensed phase current and over current peak as follows:

$$I_{ppeak} > I_0 \ldots\ldots.(9)$$

Where the peak phase current is denoted by i_p phase. The correct commutation point will have been passed if the phase current exceeds i0, at which time the phase commutation will have been ctivated. If the phase current is smaller than the over current peak, the internal and commutation times are hen compared. The commutation switching is completed right away once the internal time has crossed the commutation time.Depending on the size of the phase current, this commutation and acceleration mechanism speeds up the PMBLDC motor. Duringsensor less beginning, the PMBLDC motor is accelerated and commutated using the standard align and start method in line with apredefined commutation sequence, which results in inappropriate e commutation and a significantfirst-rush current. The whole flowchart of this opening operation is shown in **Fig. 5.** Correct commutation also considers the processor internal time (T internal) as well as the phase commutation time (T-phase).
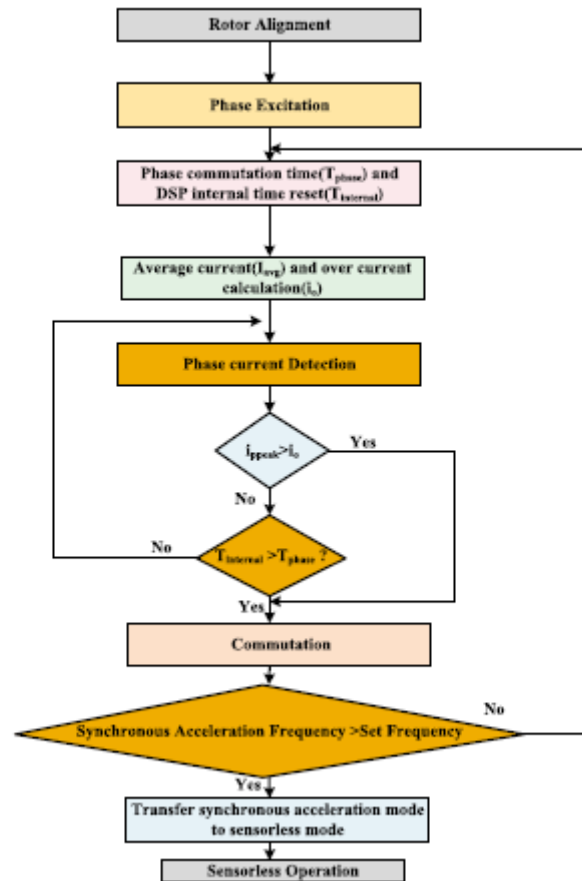
Fig.5. Peak current detection based sensorless starting method

4.3. Design of Low-Pass Filter

Due to freewheeling diode conduction, voltages on the line observed for the position sensor-less commutation estimate exhibit unwanted commutation ripple.The phase back EMFs derived from the line voltages also contain the ripples of the line voltage andswitching elements with a high frequency. During the sensor less position estimate procedure, this ripple content causes incorrect zero detection and results in an inaccurate electrical commutation. When employing first-order LPF for position estimation and electrical commutation, the spike and high frequency element are avoided. The right cutoff frequency must be chosen while creating an LPF. The system has substantial phase lag when the LPF's cutoff frequency is low, and the opposite is true when it is high because the filtered signal contains high frequency components, which again results in incorrect position recognition and incorrect commutation switching. Due to the motor's rated speed of 3000 r/min, the system frequency for this application is 100 Hz.
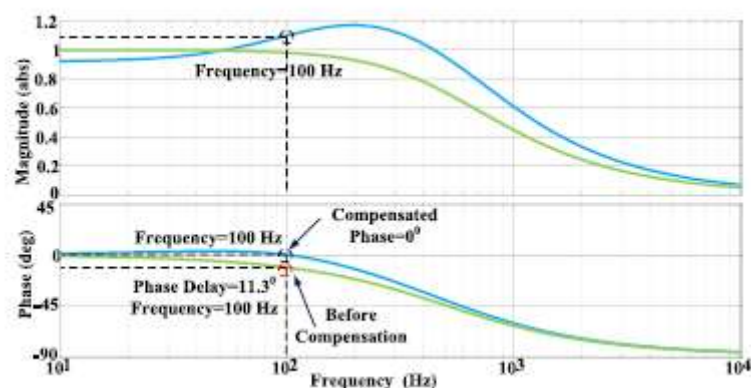

Fig.6. Magnitude and phase plot after compensation in phase.

The cutoff frequency of the LPF is designed to prevent a high cutoff frequency component from passing through at either a very low or very high cutoff frequency, which would result in a considerable phase lag in the system. A detailed control analysis and Bode plot are used to set the LPF's cutoff frequency at 500 Hz. The corresponding Bode plot is shown in Fig. 6. The relevant transfer function is identified as follows:

$$H_1(S) = \frac{\omega_c}{S+\omega_{c\omega}} = \frac{3141.6}{S+3141.6} \ldots\ldots\ldots(10)$$

WhereWcis filter cutoff frequency in rad/s. For used commercial PMBLDC motor drivesthe created filter is digitally applied in the TMS320F28377S processor. For the use of digital technology to LPF, the measured line voltages are sampled at 19.2 kHz, and the transfer function (10) is converted to a discrete z-domain. [20].this z-domain function is equivalent to

$$H_1(Z) = \frac{0.09337}{Z-0.9066} \ldots\ldots\ldots\ldots(11)$$ According to the Bode diagram in Figure 6,

the LPF causes an 11.3° phase lag in the system. The phase compensator is introduced to the system to correct the aforementioned phase lag and determine the right sensorless location.

4.4. Phase Compensator Design

To fix the phase lag that the LPF generated, a phase lead compensation was developed and installed to the system. The Bode curve in Fig. 6 shows that the LPF introduces an 11.3° phase lag. Due to the mistake in commutation caused by the lag in the anticipated back EMFs, the torque and current experience excessive ripple. Because the stator windings are heated more, the peaky phase current shortens their lifetime. With increasing motor speed, the commutation error also increases. In order to properly compensate for phase lag, the phase lag compensator is therefore crucial. The specific concepts for the phase lead compensator and its implementation using digital technology are covered in

$$G(s) = k\frac{S+\omega_1}{S+\omega_2} \qquad\ldots\ldots\ldots\ldots\ldots(12)$$

Where, ω_1 and ω_2 are the zero crossover and phase crossover frequency and k is magnitudeconstant. From the Bode plot shown in **Fig. 6,** the phase lag angle = 11.30. The magnitude constant k is determined as

$$K=\frac{1+sin\theta}{1-sin\theta} \qquad\ldots\ldots\ldots\ldots(13)$$

Phase crossover frequency is calculated as

$$\omega_1 = \frac{1}{KT}, \omega_2 = \frac{1}{T} \qquad\ldots\ldots\ldots\ldots\ldots (14)$$

Where T is the time constant. The phase compensator transfer function is

$$G(s) = 1.487\frac{S+515.25}{S+766.189} \qquad\ldots\ldots\ldots\ldots(15)$$

The aforementioned transfer function (15) is transformed the use of discrete time into the Tustin approximation and 19.2-kHz sampling rate for digital implementation of the phase compensator in the digital signal processor (DSP)

$$G(s) = \frac{1.42z-1.37}{z-0.9545} \qquad\ldots\ldots\ldots\ldots(16).$$

5. Proposed Method
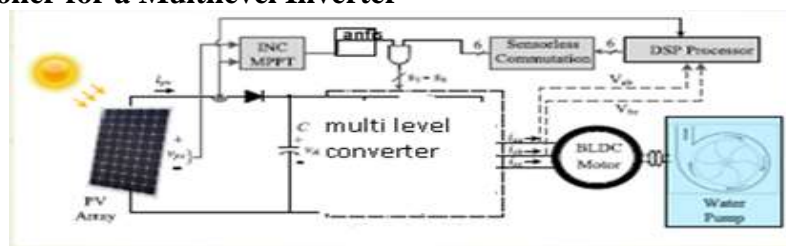## 5.1. ANFIS Controller for a Multilevel Inverter

Fig.7. System Configuration of position sensorless brushless DC Motor drive

In this technique,we are using 5-level cascade multi-level inverter in place of three phase voltage source inverter shown in fig .7, why in fact to use MLI because VSC has poor effeciency in medium

and high voltage applications,maily power loss across switches .Hence to reduce this problem MLI used .As number of levels in MLI increase ,THD will be reduce and getting pure sinusodial wave form but the power modules increased. This leads to complexity between switch and power supply . Hence ,this work proposed a 5-level MLI with reduced switches. In cascade 5-level MLI include 2-H bridge , 8 IGBT switches are to produce output is shown in fig,
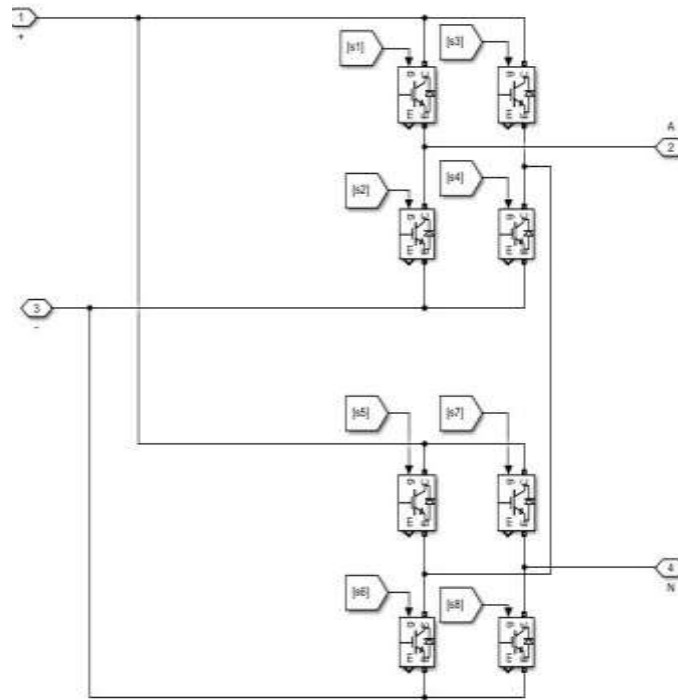

Fig.8. 5-level cascade H-bridge

5.2 ANFIS Controller

The modelling, regulating and estimating parameters in complicated systems, ANFIS is used. ANFIS is a system that combines fuzzy inference with artificial neural networks (ANNs) (FIS).The advantages of combining ANN with fuzzy-set theory outweigh their respective drawbacks. Without depending entirely on expert information necessary for a fuzzy logic model, the ANFIS model may be taught. The benefit of possessing both verbal and numerical data is provided by the ANFIS model. ANFIS also makes use of the ANN's ability to classify data and identify patterns.The ANFIS model is less likely to result in memory mistakes and is more transparent to the user than the ANN. As a result, the ANFIS has a number of benefits, including the ability to adapt, the nonlinearity of the system, and the potential for quick learning.

This method effectively creates a fuzzy logic model with rules that are built while the model is being trained. Data is the basis for the training process. The training examples are used by ANFIS to create a fuzzy inference system (FIS) whose membership function parameters are taken from them. Mamdani and Sugeno are the two most often utilized fuzzy inference methods. The fundamental distinction between Mamdani and Sugeno is that the Sugeno system's output membership functions are either linear or constant. The Mamdani system, however, allows for the output membership functions to be triangular, Gaussian, etc. As opposed to the Mamdani type, the Sugeno type fuzzy inference system is more computationally efficient, hence it was chosen in this investigation. The Mamdani type relies more heavily on subject-matter expertise. But actual data is used to train the Sugeno type.

For the sake of comprehending the ANFIS architecture, we presummated that there are two inputs: x and y. Two fuzzy if-then rules may be expressed as follows for a Sugeno fuzzy model of first order:

Rule 1: f1 = p1x + q1y + r1 if x is A1 and y is B1.

Rule 2: f2 = p2x + q2y + r2 if x and y are A2 and B2, respectively.

Where p1, q1, r1, during the training phases. While A1and B1 fuzzy sets, f1 and f2 is output. The two rules' respective ANFIS architectures are displayed in**Fig. 9.**

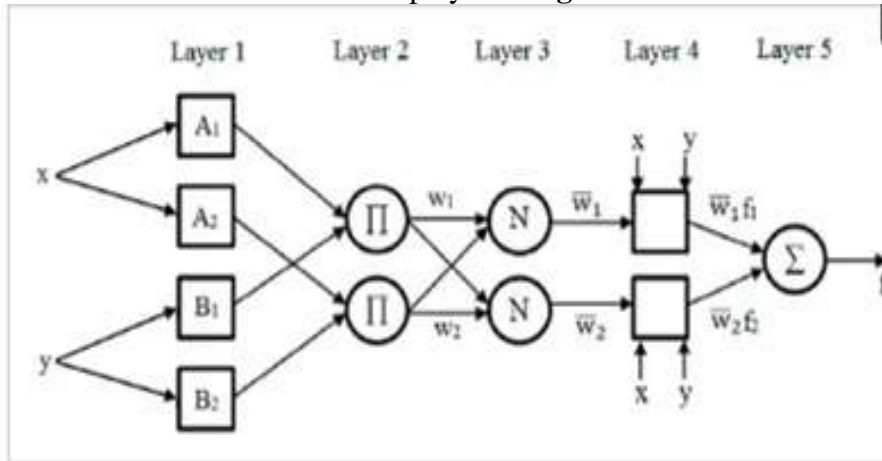**Fig.9.** The architecture of the adaptive neuro-fuzzy inference system (ANFIS) model with two inputs, one output and two rules.
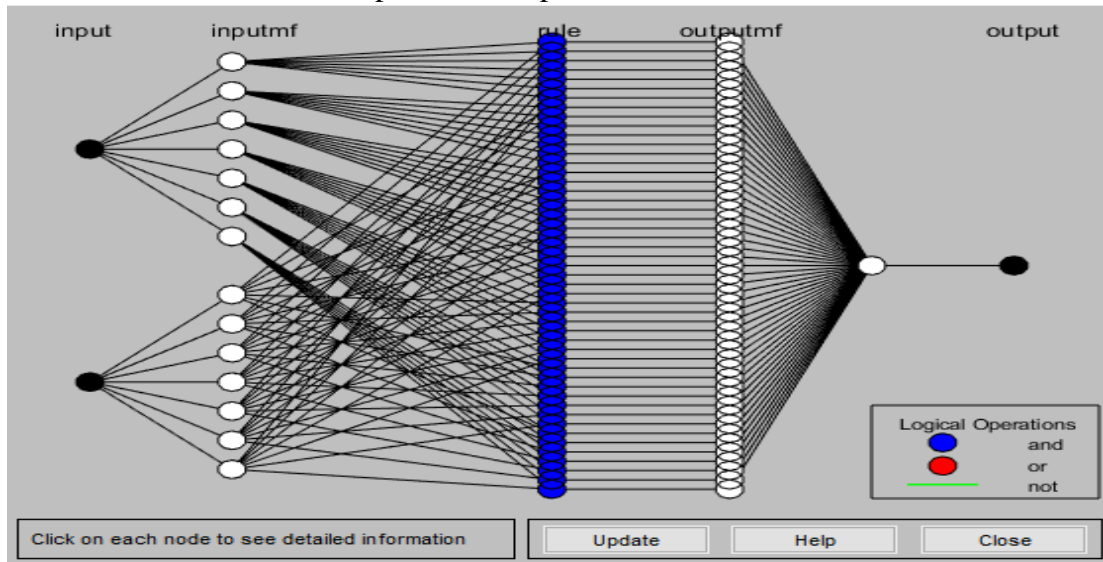

Fig.10. Structure of ANFIS

6. SIMULATION RESULTS

MATLAB is used to simulate this position sensor less control of a water pump powered by BLDC motors. From 1000 to 500 W/m2, different sun insolation levels are used during the experiment. This part evaluates and displays the beginning steady-state and dynamics performances. The system's performance has been demonstrated by the examined parameters to be adequate and steady.
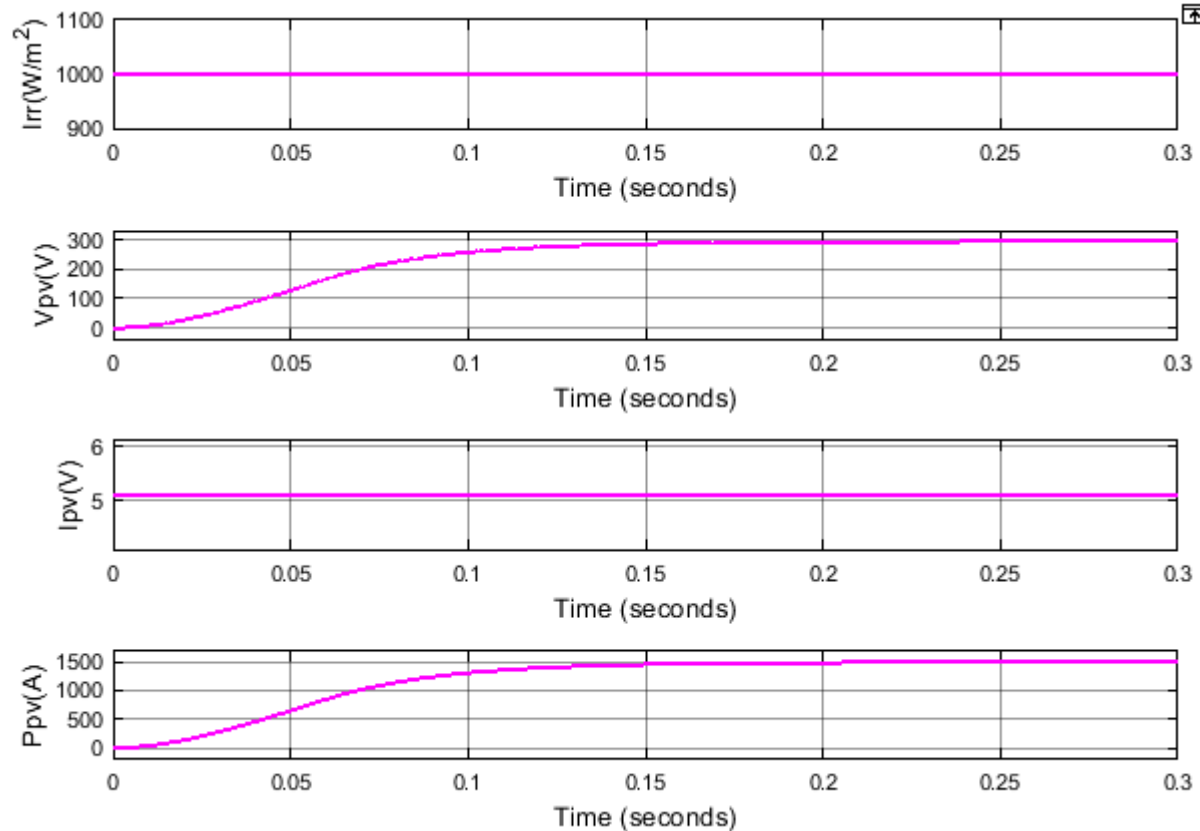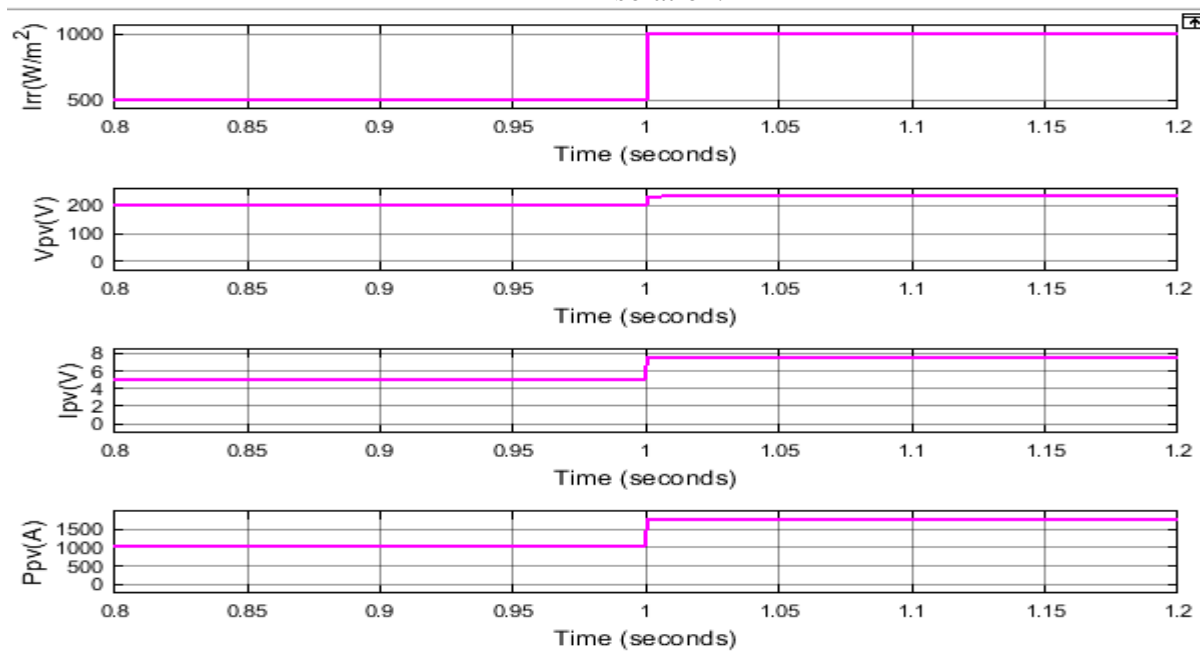
Fig. 11. Solar PV array performance. (a) Steady-state and starting performance at 1000 W/m2 insolation.

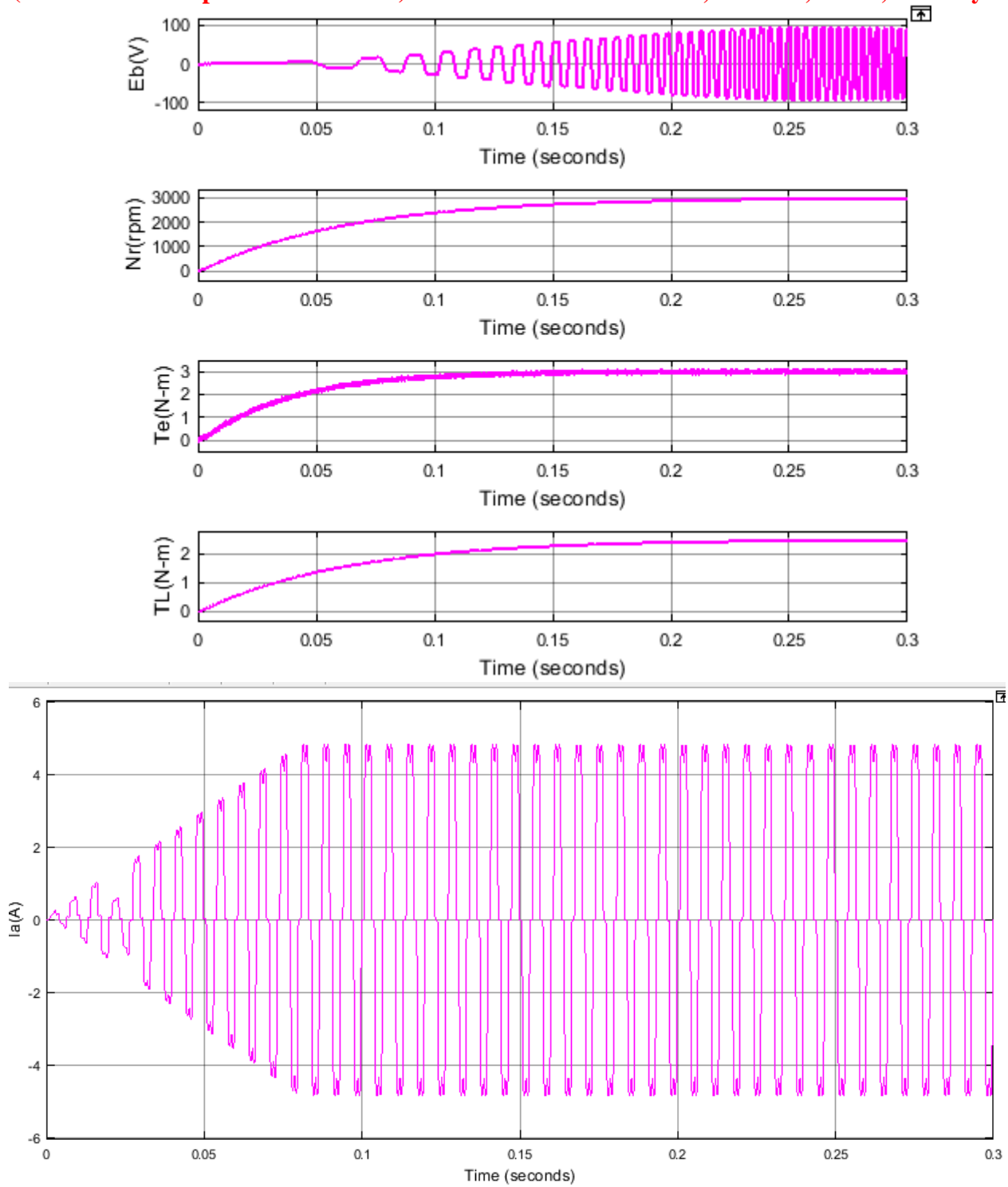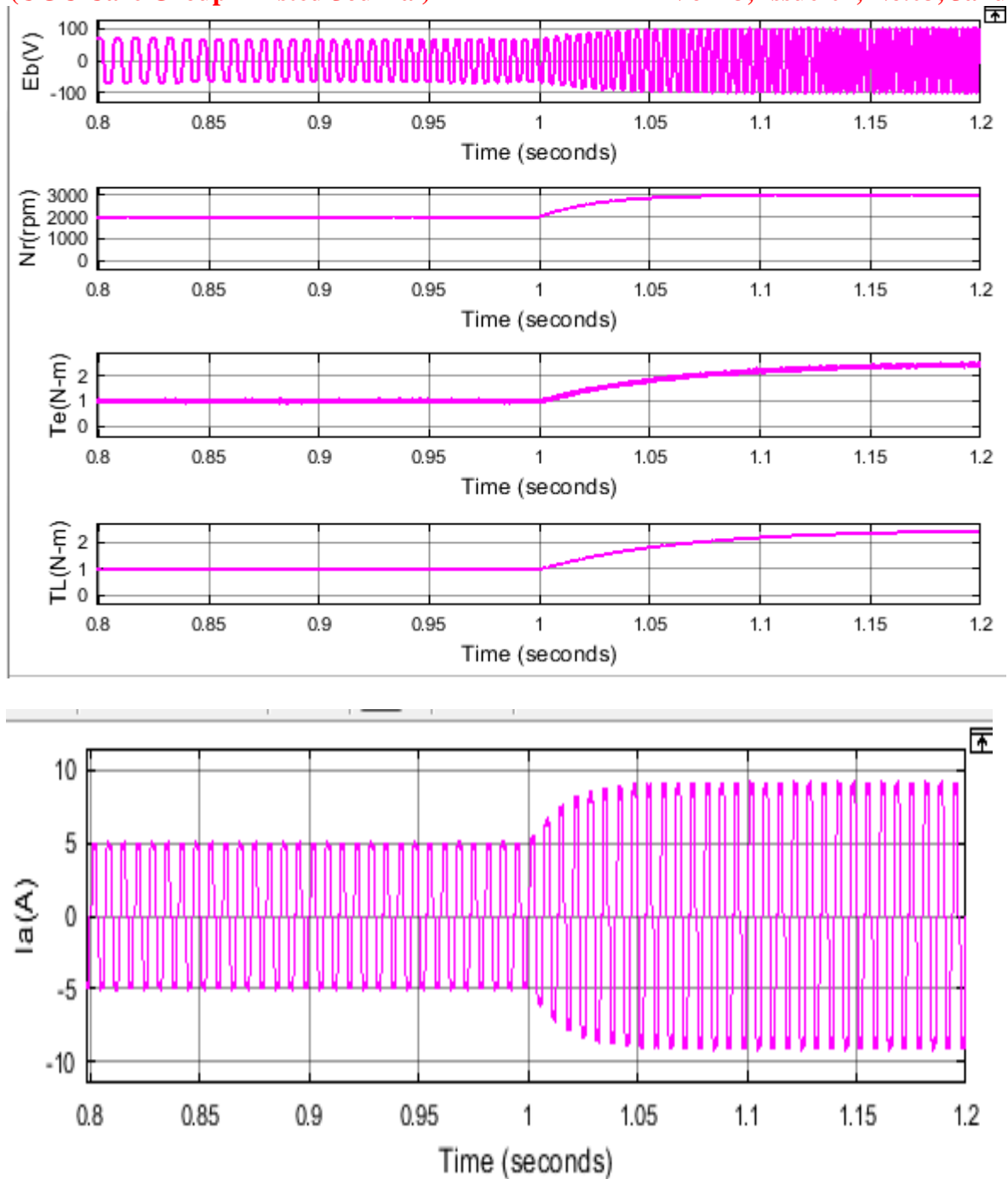(b) Dynamic performance varying from 500 to 1000 W/m2.

Fig. 12. BLDC motor performance at sensorless scheme. (a) Zero starting and steady-state performance at 1000 W/m2 irradiance.

(b) Dynamic performance varying from 500 to 1000 W/m2 irradiance.
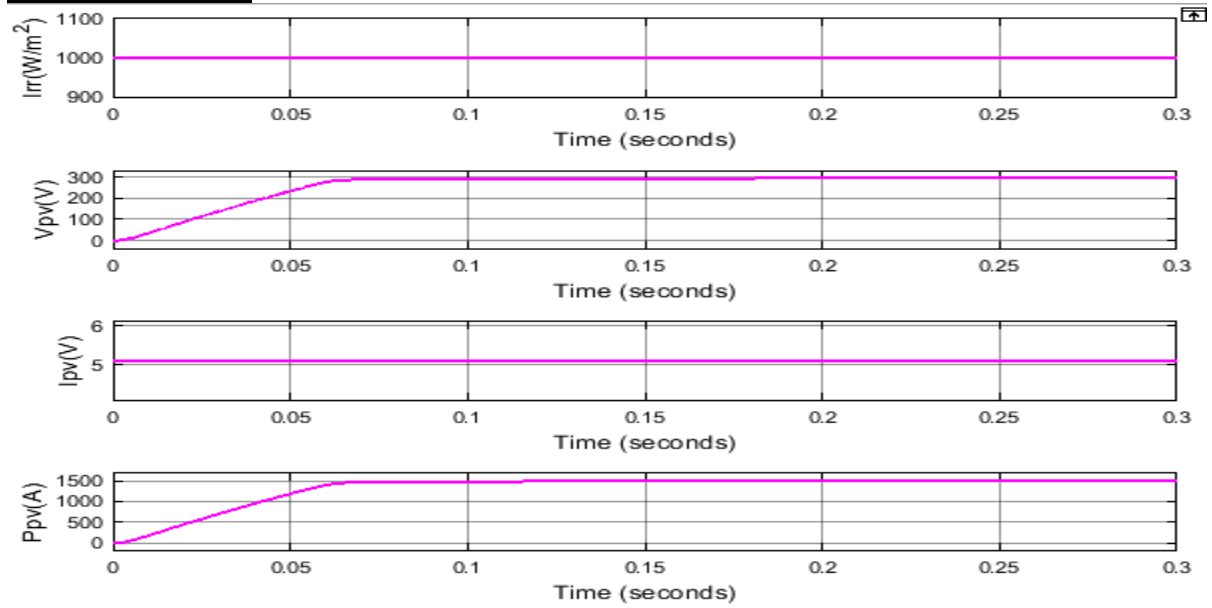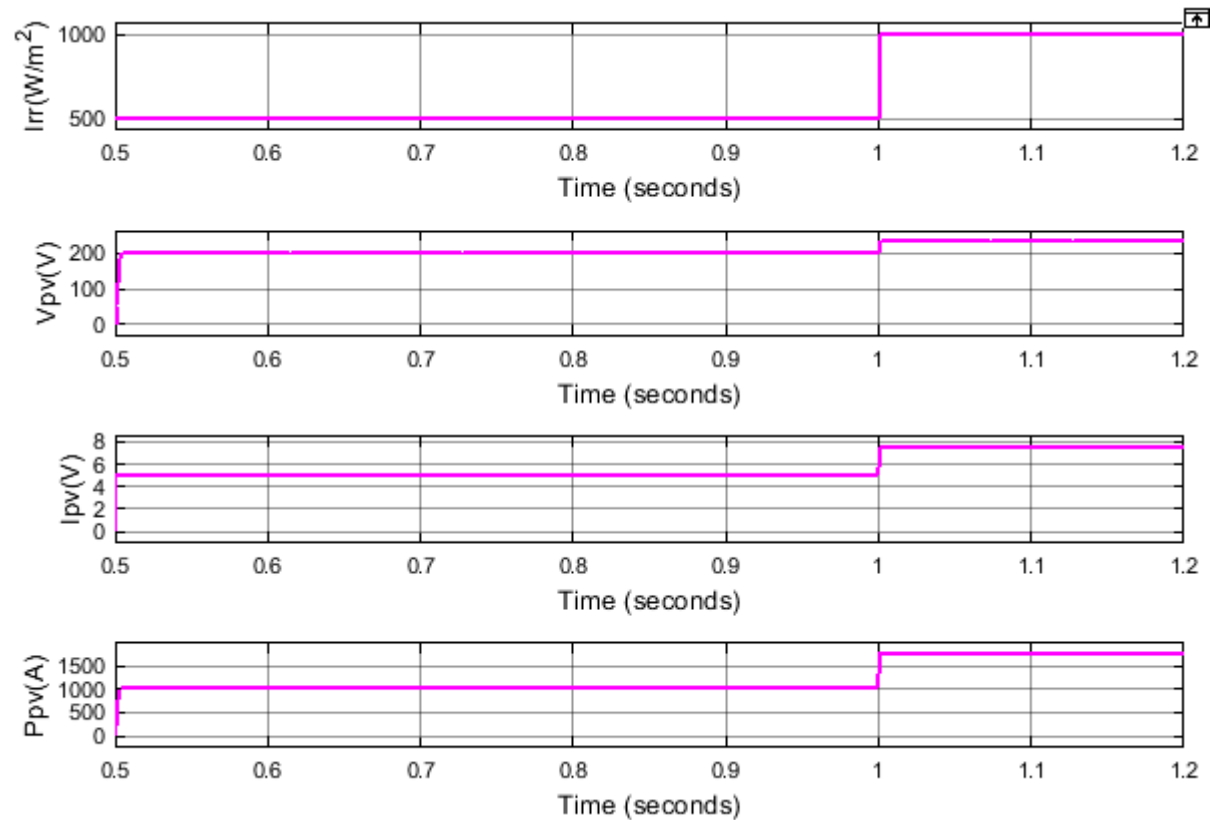
Extension results:

Fig. 13. Solar PV array performance. (a) Steady-state and starting performance at 1000 W/m2 insolation.

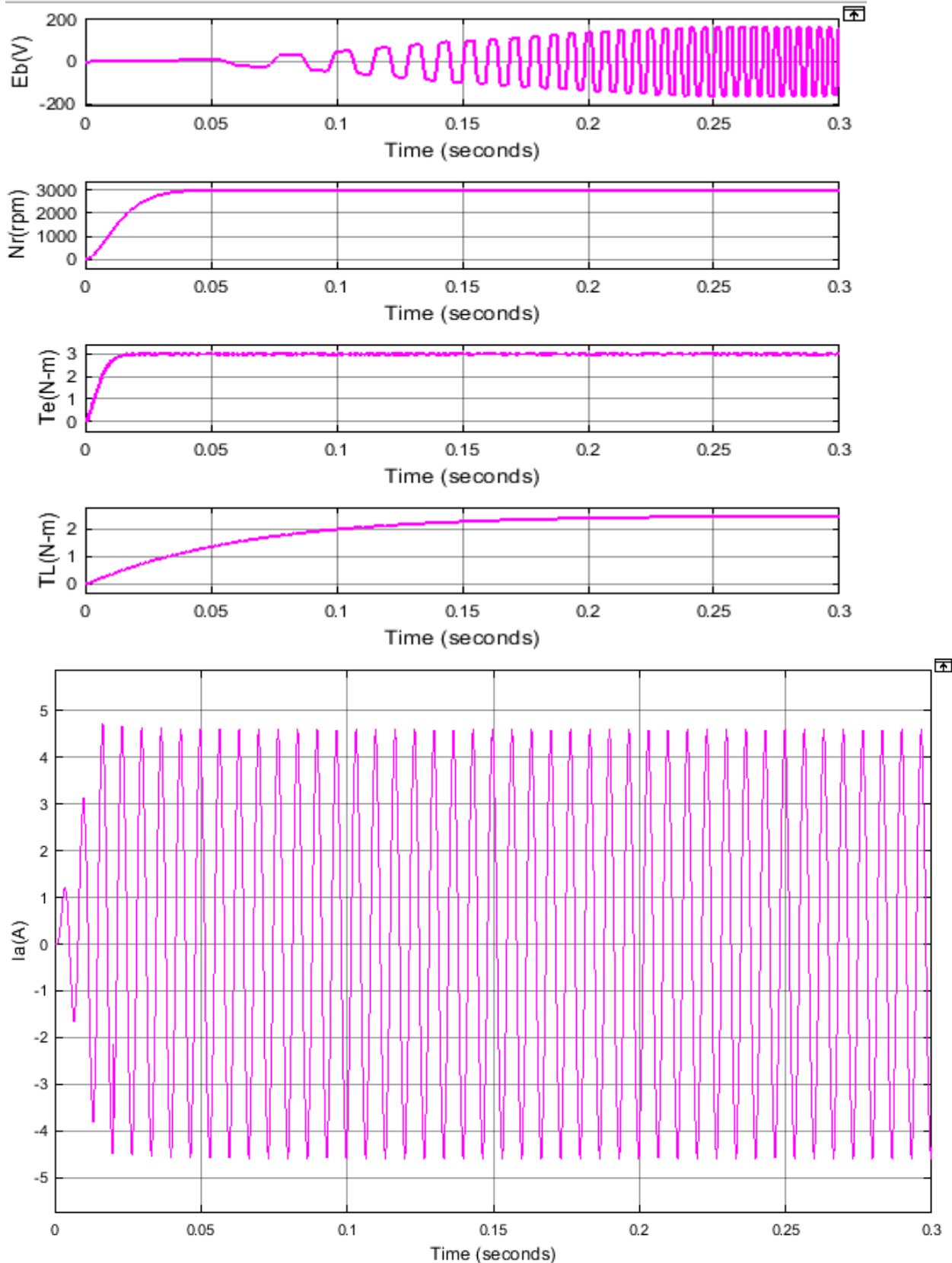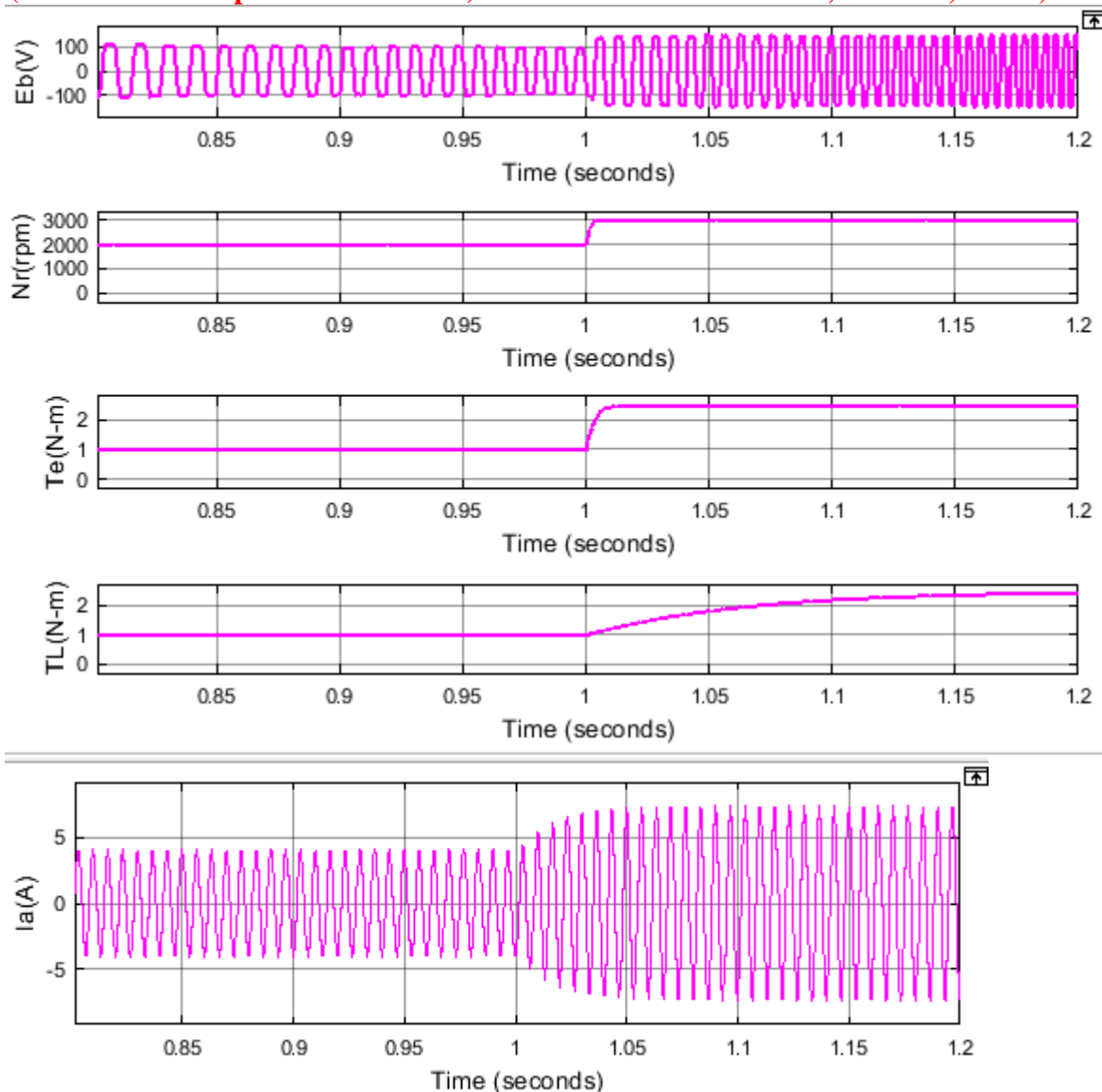(b) Dynamic performance varying from 500 to 1000 W/m2.

Fig. 14. BLDC motor performance at sensorless scheme. (a) Zero starting and steady-state performance at   1000 W/m2 irradiance.

(b) Dynamic performance varying from 500 to 1000 W/m2 irradiance.

7. CONCLUSION

This project proposes,5-level multi-level cascade H-bridge with ANFIS controller, A smooth start, reliable position sensor less control, and beginning peak current management of a PMBLDC motor have all been described for solar-powered pumping. In order to extend the lifespan of the drive and PMBLDC motor, the starting approach being used minimizes the high starting inrush current. The system is more inexpensive and small as a result of the usage of fewer position sensors. Utilizing simulation findings, the designed drive's dependability and robustness are verified. The performance and efficiency of the solar MPPT and PMBLDC motor are included in the same data that was collected using DSO. For the solar MPPT, more than 99% efficiency is anticipated. Using this method ,fluctuations in reduced successfully.

REFERENCES

[1] A. Sen and B. Singh, "Peak current detection starting based position sensorless control of BLDC motor drive for PV array fed irrigation pump," in Proc. IEEE Int. Conf. Environ. Elect. Eng. Ind. Commercial Power Syst. Europe (EEEIC /I&CPS Europe), 2019, pp. 1–6.

[2] S. Jain, A. K. Thopukara, R. Karampuri, and V. T. Somasekhar, "A single-stage photovoltaic system for a dual-inverter-fed open-end winding induction motor drive for pumping applications," IEEE Trans. Power Electron., vol. 30, no. 9, pp. 4809–4818, Sep. 2015.

[3] L. An and D. D. Lu, "Design of a single-switch DC/DC converter for a PV-battery-poweredpumpsystemwithPFM+PWMcontrol," IEEE Trans. Ind. Electron., vol. 62, no. 2, pp. 910–921, Feb. 2015.

[4] J. V. M. Caracas, G. d. C. Farias, L. F. M. Teixeira, and L. A. d. S. Ribeiro, "Implementation of a high-efficiency, high-lifetime, and low-cost converter for an autonomous photovoltaic water pumping system," IEEE Trans. Ind. Appl., vol. 50, no. 1, pp. 631–641, Jan./Feb. 2014.

[5] T.-H. Kim and M. Ehsani, "Sensorless control of the BLDC motors from near-zero to high speeds," IEEE Trans. Power Electron., vol. 19, no. 6, pp. 1635–1645, Nov. 2004.

[6] S. Dusmez, A. Khaligh, M. Krishnamurthy, E. Ugur, and M. Uzunoglu, "Sensorless control of BLDCs for all speed ranges with minimal components," in Proc. Inter. Aegean Conf. Elect. Machines Power Electron. Electromotion, Joint Conf., 2011, pp. 626–631.

[7] J. Park, S. Hwang, and J. Kim, "Sensorless control of brushless DC motors with torque constant estimation for home appliances," IEEE Trans. Ind. Appl., vol. 48, no. 2, pp. 677–684, Mar./Apr. 2012.

[8] J. Feng, K. Liu, and Q.Wang, "Scheme based on buck-converter with three phase H-bridge combinations for high-speed BLDC motors in aerospace applications," IET Electric Power Appl., vol. 12, no. 3, pp. 405–414, Mar. 2018.

[9] A. Ahfock and D. Gambetta, "Sensorless commutation of printed circuit brushless direct current motors," IET Electric Power Appl., vol. 4, no. 6, pp. 397–406, Jul. 2010.

[10] R. Kumar and B. Singh, "Buck-boost converter fed BLDC motor drive for solar PV array based water pumping," in Proc. IEEE Inter. Conf. Power Electron., Drives Energy Syst. (PEDES), 2014, pp. 1–6.

[11] G. N. A. Maranhão, A. U. Brito, J. T. Pinho, J. K. S. Fonseca, A. M. Leal, and W. N. Macêdo, "Experimental results of a fuzzy controlled variablespeed drive for photovoltaic pumping systems: A review," IEEE Sensors J., vol. 16, no. 9, pp. 2854–2864, May 2016.

[12] B. Singh and R. Kumar, "Simple brushless DC motor drive for solar photovoltaic array fedwater pumping system," IET Power Electron., vol. 9, no. 7, pp. 1487–1495, 2016.

[13] S. Sheik Mohammed, D. Devaraj, and T. P. Imthias Ahamed, "Maximum power point tracking system for stand alone solar PV power system using adaptive neuro-fuzzy inference system," in Proc. Biennial Inter. Conf. Power Energy Syst.: Towards Sustain. Energy (PESTSE), 2016, pp. 1–4.

[14] A. Gupta, P. Kumar, R. K. Pachauri, and Y. K. Chauhan, "Performance analysis of neural network and fuzzy logic based MPPT techniques for solar PV systems," in Proc. 6th IEEE Power India Inter. Conf. (PIICON), Delhi, India, 2014, pp. 1–6.

[15] K. Lee, D. Kim, B. Kim, and B. Kwon, "A novel starting method of the surface permanent-magnet BLDC motors without position sensor for reciprocating compressor," IEEE Trans. Ind. Appl., vol. 44, no. 1, pp. 85–92, Jan./Feb. 2008.

[16] R. Kumar and B. Singh, "Single stage solar PV fed brushless DC motor driven water pump," IEEE J. Emerg. Sel. Top. Power Electron., vol. 5, no. 3, pp. 1377–1385, Sep. 2017.